


RESEARCH

Open Access



Application of fluidized-bed homogeneous crystallization technology to carbon sequestration and recovery from flue gas

Po-Chun Huang¹, Anabella C. Vilando², Thi-Hanh Ha¹ and Ming-Chun Lu^{1*} 

Abstract

The Earth's energy balance produced by human activity is the main factor in the complex relationship between greenhouse gases and global warming. The Taiwan Environmental Protection Agency reports that carbon dioxide makes up more than 95% of Taiwan's most recent greenhouse gas emissions. This study used fluidized-bed homogeneous crystallization (FBHC) technology to recover carbonate in a simulated CO₂-enriched flue gas. It was specifically designed to determine how carbonate removal and crystallization efficiency were affected by carbonate surface loading, the influence of the source of calcium ions, and interfering substances. Results revealed that the best surface loading at 55 kg m⁻² h⁻¹ achieved 93% removal and 84% crystallization efficiency. At 50 mg L⁻¹ of sulfate ions, the presence of more interfering compounds tends to reduce carbonate removal to 97% and 91% crystallization. Regarding X-ray diffraction data, the recovered carbonate crystals resembled calcium carbonate crystals. It has been demonstrated that carbonate can be recovered using FBHC technology as a method of CO₂ capture and storage.

Keywords Calcium carbonate, Carbon dioxide capture, Surface loading, Sulfate ions, Global warming

1 Introduction

Climate forcing is a change in the Earth's energy balance that ultimately has a warming or cooling effect. As a result of warming or positive climate forcing, the atmospheric concentration of greenhouse gases (GHG) increases. Between 1990 and 2019, the total amount of heat from GHG that humans have emitted to the Earth's atmosphere grew by 45%. Carbon dioxide (CO₂) alone increased the warming effect by 36% [1]. Carbon dioxide is the main greenhouse gas, trapping heat and

contributing to Earth's warmth. Unlike oxygen and nitrogen, CO₂ and other GHG prevent Earth from freezing by reflecting heat to the surface [2]. By adding more carbon dioxide to the atmosphere, people are supercharging the natural greenhouse effect, causing global temperature to rise [2]. Human activities have increased CO₂ levels, enhancing the natural greenhouse effect and causing global warming. From the 1960s to 2022, fossil fuel emissions rose from about 11 to 36.6 Gt of CO₂ according to Global Carbon Budget 2022 [3]. This surge has led to around 1 °C of global warming, potentially reaching 1.5 °C soon if it continues to increase at the current rate [4]. The Kyoto Protocol operationalizes the United Nations Framework Convention on Climate Change by requiring industrialized nations and economies in transition to set and achieve individual emission reduction targets for GHG [5]. The Earth's surface warms when CO₂

*Correspondence:

Ming-Chun Lu
mmclu@nchu.edu.tw

¹Department of Environmental Engineering, National Chung Hsing University, Taichung City 40227, Taiwan

²College of Engineering and Architecture, Bicol State College of Applied Sciences and Technology, Naga City 4400, Philippines



© The Author(s) 2024. **Open Access** This article is licensed under a Creative Commons Attribution 4.0 International License, which permits use, sharing, adaptation, distribution and reproduction in any medium or format, as long as you give appropriate credit to the original author(s) and the source, provide a link to the Creative Commons licence, and indicate if changes were made. The images or other third party material in this article are included in the article's Creative Commons licence, unless indicated otherwise in a credit line to the material. If material is not included in the article's Creative Commons licence and your intended use is not permitted by statutory regulation or exceeds the permitted use, you will need to obtain permission directly from the copyright holder. To view a copy of this licence, visit <http://creativecommons.org/licenses/by/4.0/>.

concentration rises due to the atmosphere's increased capacity to trap heat [6]. Decarbonization efforts in the energy and industrial sectors are essential to achieving the net-zero GHG emissions target by 2050 [7]. The current human involvement is connected to the annual generation of over 40 Gt of CO₂, primarily due to the reliance on fossil fuels for energy, with CO₂ released from industrial processes accounting for 78% of the growing global greenhouse gas emissions [8]. Utilizing captured CO₂ for chemical production or safe disposal is being explored, with carbon mineralization as a proposed method.

The urgent need to combat climate change has sparked the investigation of cutting-edge technologies that can efficiently collect and store CO₂ emissions from various sources, mainly industrial processes, and power generation. These methods include carbon capture from manufacturing processes that produce product gas for carbon-capture utilization and sequestration or permanent storage underground in geological cavities (CCS) [9]. Flue gas emissions, which mostly result in the combustion of fossil fuels, contain a sizable amount of CO₂ and play a significant role in the greenhouse effect and global warming. Traditional carbon capture techniques employ liquids or solid adsorbents to trap CO₂, which can be expensive, energy-intensive, and difficult to dispose of once captured. Measures to reduce the release of CO₂ have been made, such as switching to renewable energy as well as implementing energy-saving methods. Successful CO₂ reduction depends on using CCS approaches [10].

However, the fluidized-bed homogenous crystallization (FBHC) technology for CO₂ capture and storage from flue gas emissions is a promising method. FBHC technology is a development of conventional precipitation technology. Conventional chemical precipitation precipitates an ionic compound from a bulk solution as sludge. However, these sludge products feature high water-content, which increases the cost of sludge handling [11]. Three possible stages for granulation mechanisms occurring in FBHC reactor have been suggested in Fig. 1a [12, 13], including: (a) The first stage is homogeneous nucleation, occurring in the lower part, initiated by the mixing of concentrated reactants at the inlet. This leads to reduced supersaturation and encourages crystal aggregation. (b) The second stage is heterogeneous nucleation, commonly in the middle part, where moderate supersaturation causes cations and anions to nucleate on the seed surface and form a layer. (c) The third mechanism occurs in the upper part, with low supersaturation leading to the metastable zone where crystals grow through lattice growth and become big granules. This innovative method uses fluidization and crystallization concepts to increase the effectiveness, scalability, and environmental viability of CO₂ capture. The greater scalability and adaptability

of FBHC technology makes it suitable for integration with current industrial processes and power plants. The FBHC method uses fewer chemicals and produces crystals with good yields that are larger and purer [14]. It also requires less space for the fluidized bed reactor (FBR) due to its tubular features and transforms the tiny crystals into a solid form with low moisture content (<5%). The produced crystals can be utilized as industrial materials to recycle resources, reduce waste, and lower the price of products [15]. The influx rate of the reactor converts CO₂ gathered from industrial flue gas into calcium carbonate crystals using the FBHC technology for the CCS method [10, 16]. The homogenous crystallization process requires less energy input because the crystals spontaneously form in the solvent under specific temperature and pressure conditions. Due to its high conversion efficiency, the FBHC technology is superior to other methods.

In this study, calcium was selected as a precipitant to recover carbonate anions from the solution via FBHC technology. Unlike other metal ions, calcium was shown to be an environmental-friendly precipitant and has a higher potential to form (as presented in Fig. 1b). On the other hand, calcite is a common mineral in geological and archaeological contexts. The granule of calcite is the main component of limestone, chalk, marble, travertine, and is often a major component of wind-borne sediment (loess) and cemented sediments [13]. Calcium carbonate also has many applications, such as fillers for plastics, papers, and rubbers [14]. This study aims to recover calcium carbonate crystals using FBHC technology from the flue gas carbonate absorbent solution from industrial processes. This could be a starting point for additional key parameters to study atmospheric CO₂ mitigation. Specifically, it determines the influence of (a) the surface loading of the carbonate ions, (b) the amount of calcium ion supplied in the FBR, and (c) the influence of sulfate ions as interfering solutions on the removal and recovery of CO₂ in the form of carbonate crystals. Moreover, the generated crystals from the treatment process were analyzed using Scanning Electron Microscope (SEM) for surface morphology, X-ray diffractometer (XRD) for elemental analysis, and X-ray photoelectron spectroscopy (XPS) for chemical electron analysis.

2 Materials and methods

2.1 Chemicals

The actual concentrations of the pollutants were simulated to prepare the solutions. For the flue gas liquid absorbent solution produced from carbon capture activities, potassium carbonate (K₂CO₃, 99.5%) was used. For the precipitant solution, calcium nitrate (Ca(NO₃)₂·4H₂O, 99%) and calcium hydroxide (Ca(OH)₂, 96%) were the sources of calcium ions. To adjust the pH of the solution, nitric acid (HNO₃, 69–71%) and sodium

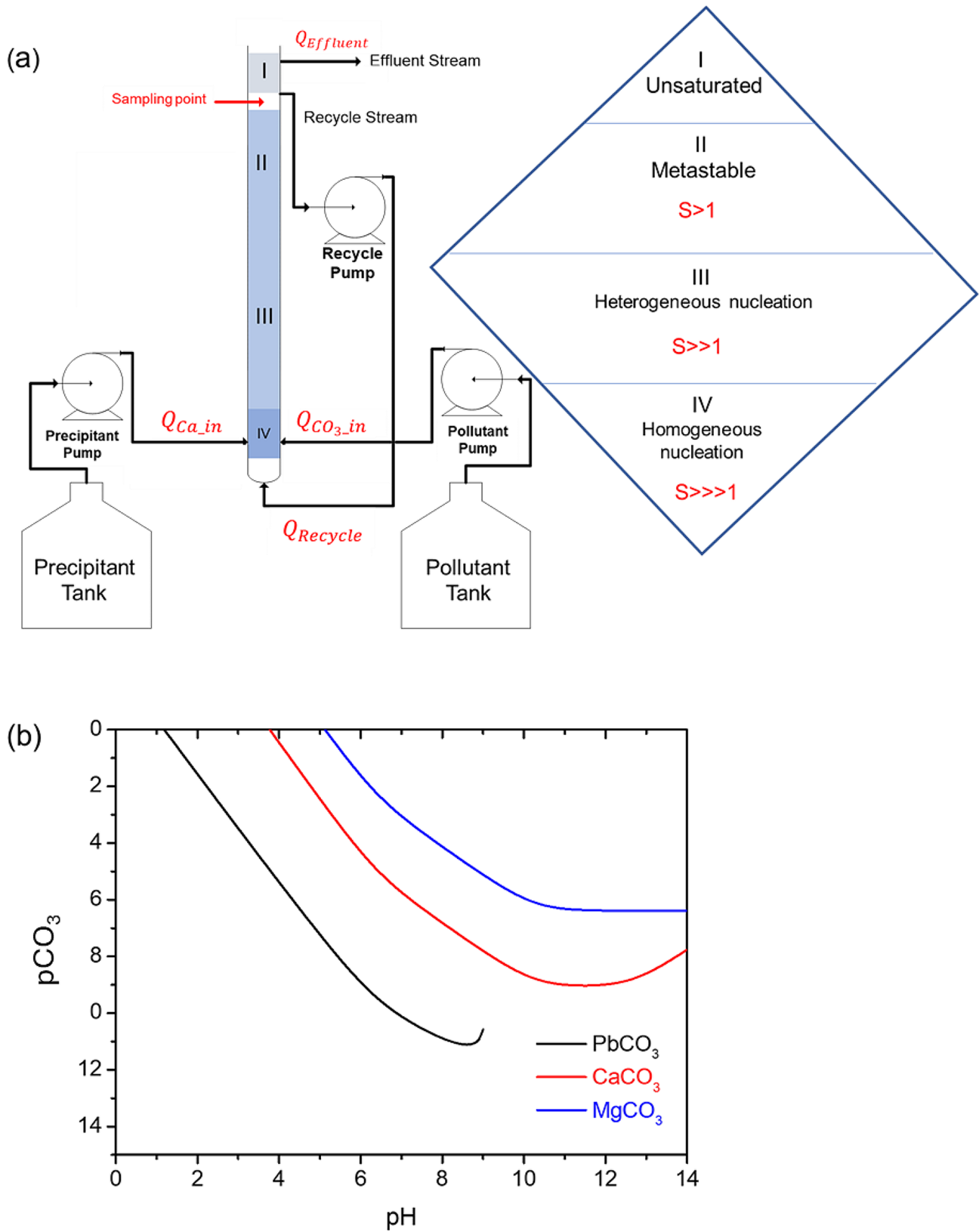
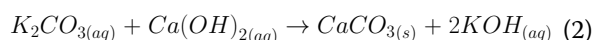
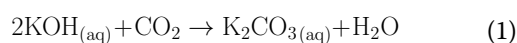


Fig. 1 (a) Fluidized-bed homogeneous crystallization apparatus; (b) the solubility curve of various metal carbonate ($[CO_3^{2-}] = 0.02\text{ M}$, $[Metal]/[Carbonate]$ MR = 1/1)

hydroxide (NaOH, 95%) were utilized. All chemicals were purchased from Lian Gong Chemicals with an analytical grade, and no purification was done. All solutions were freshly prepared using ultra-pure reverse osmosis water and deionized at a resistivity of 18.2 MΩ cm.

2.2 The FBR setup

This process consists of a two-stage CO₂ capture utilizing CO₂ as the gas and a potassium hydroxide (KOH) solution as the absorbent for converting to calcium carbonate crystals. The two-stage system of crystallization and CO₂ absorption is best characterized by chemical processes, as shown in Eqs. (1) and (2).



It has been thoroughly investigated that KOH has a large capacity for CO₂ absorption [17]. This study focused on

the second-phase reaction to crystallize the calcium carbonate in the system. The synthetic carbonate source utilized in the FBR was a K₂CO₃ solution as a source of CO₂.

The FBR comprised a glass cylinder with a total volume of 450 mL, composed of two parts (Fig. 2). The upper region is the effluent region with dimensions of 20 cm in height and 4 cm in diameter. The lower region is the reaction region and has dimensions of 80 cm in height and 2 cm in diameter, respectively. The rapid expansion lowered the flow rate from the reaction region to the effluent region. Simulated flue gas wastewater and precipitant solution were fed continuously into the reactor. The recirculation flow rate was adjusted to ensure uniform flow distribution throughout the reactor. At the bottom of the FBR, glass beads with a diameter of 0.5 cm were stacked at a height of 4 cm to ensure an even distribution of flows inside the FBR. Three (3) inlets at the bottom of the FBR were linked to a peristaltic pump (Masterflex L/S, Cole-Parmer Instrument, USA) for the pollutant solutions, precipitants, and reflux flows. To monitor the pH of the

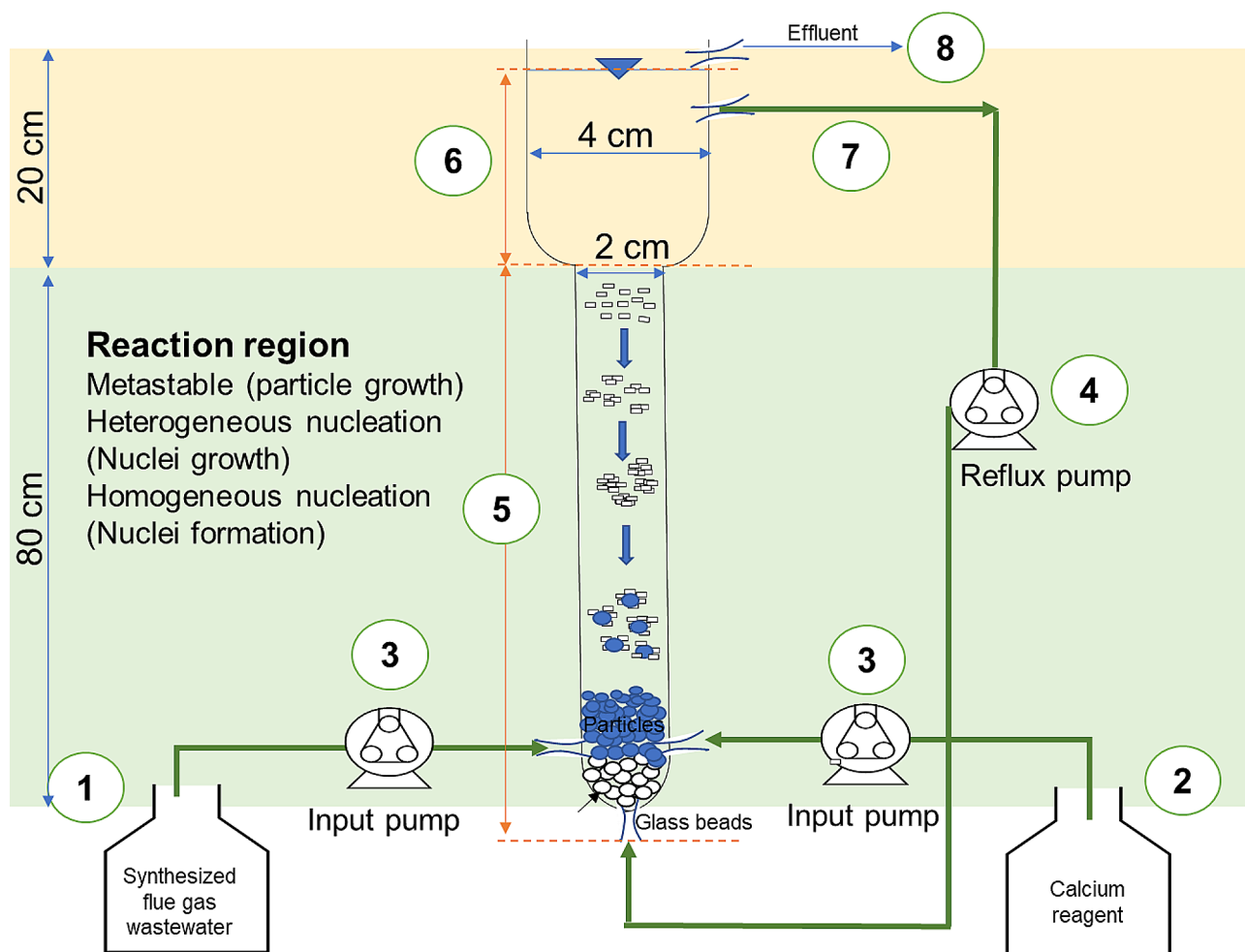


Fig. 2 The FBHC technology setup. (1) Synthesized flue gas wastewater, (2) calcium ion reagent, (3) peristaltic pumps, (4) recirculation pump, (5) reaction region, (6) effluent region, (7) recirculation flow, (8) treated effluent discharge

Table 1 Experimental parameters for calcium carbonate crystallization in FBHC

Symbol	Definition	Equation
Q_{CO_3}, Q_{Ca} (mL min ⁻¹)	Influx of CO ₃ ²⁻ -containing wastewater and Ca solution, respectively	
$(CO_3^{2-})_{in}$ (M)	The influent concentration of CO ₃ ²⁻	
$(CO_3^{2-})_t, (CO_3^{2-})_d$ (M)	Total and soluble of carbonate in effluent	
A (cm ²)	Cross-section area of reactor	
V_T (mL)	The total volume of the reaction solution in the reactor	
L (kg m ⁻² h ⁻¹)	Cross-section loading	$\frac{C_{CO_3} Q_{CO_3}}{A}$
Q_T (mL min ⁻¹)	Total influx flow rate	$Q_{CO_3} + Q_{Ca}$
HRT (min)	Hydraulic retention time	$\frac{V_T}{Q_T}$

Table 2 Specific experiment design of study

Run	Variables	Levels	Constant conditions		
			Carbonate concentration (mM)	[Ca ²⁺]/[CO ₃ ²⁻] MR	pH
1	Surface loading (kg m ⁻² h ⁻¹)	14, 21, 34, 55, 62, 69	-	1/1	10
2	[Ca ²⁺]/[CO ₃ ²⁻] MR	0.9, 0.95, 1.0, 1.05, 1.1	0.096	-	10
3	Sulfate concentration (mg L ⁻¹)	0, 10, 20, 30, 40, 50	0.096	1/1	10

discharging solution, a pH/ORP meter (Shin-Shang Tech Instruments Co., PC-310) was mounted at the effluent region. The experimental parameters of the FBR reactors are listed in Table 1.

2.3 Experimental procedures and analytical techniques

2.3.1 Experimental procedures

The source of the synthetic flue gas wastewater containing CO₂ was simulated according to its composition. The design data for the necessary absorption tower parameters were created based on the existing plant design. The flue gas contains 15% CO₂, simulating that from fossil fuel and thermal plants [18, 19]. The CO₂ absorption efficiency was estimated to be 90%, and the carbonate concentration in the leaving streams of the absorption tower was about 0.33 M. The synthetic flue gas wastewater with CO₂ was initially fed into the reactor at 10 mL min⁻¹, increasing by 10 mL min⁻¹ every 6 h until reaching 50 mL min⁻¹. A 1:1.3 molar ratio (MR) of Ca(OH)₂ to carbonate solutions was added to 20 L tanks, and NaOH was used to adjust the pH by adding in CO₃²⁻ containing wastewater. Ca²⁺ and CO₃²⁻ at concentrations of 0.024 and 0.018 M, respectively, were pumped into the FBR at equal rates, with recirculation flow varying between 10 and 50 mL min⁻¹. The fluidization state was confirmed by keeping formed granules at less than 50% bed expansion in the fluidized-bed reactor. The FBHC process did

not use external seeds for crystallization; instead, a preliminary stage allowed for seed formation within the reactor until precipitates were stable enough to resist washout. The pH was kept between 10.0 and 10.3 using NaOH and HCl. Experiments, done in triplicate at room temperature [20], ran continuously for seven days, which was sufficient for consistent carbonate removal and precipitate stabilization as per preliminary studies. The experimental design is detailed in Table 2.

At the effluent region of the FBR, two (2) samples of ten (10) mL each were taken out and placed in a sample bottle for analysis. The first sample was filtered with 0.45 μm microfilter membrane (GHP, PALL™), while the other was not. Both were acid-treated using HNO₃ (69% v/v) to terminate the reactions. The dissolved carbonate ions in the filtrate were examined to determine the effectiveness of carbonate removal. In Eq. (3), the carbonate ion removal efficiency was demonstrated using the ratio of carbonate ions removed in the FBR to all carbonate ions initially present in the flue gas wastewater solution.

$$\%Removal = \left[\frac{(CO_3^{2-})_{in} - (CO_3^{2-})_{out}}{(CO_3^{2-})_{in}} \right] \times 100 \quad (3)$$

The amount of total carbonate ions required to achieve the crystallization effects is shown in Eq. (4). For the unfiltered sample, the crystallization efficiency was assessed. The reaction between the carbonate precipitant and the calcium ion resulted in the formation of large crystals.

$$\%Crystallization = \left[\frac{(CO_3^{2-})_{in} - (CO_3^{2-})_t}{(CO_3^{2-})_{in}} \right] \times 100 \quad (4)$$

The carbonate concentration at the inlet was named $(CO_3^{2-})_{in}$. Meanwhile $(CO_3^{2-})_{out}$ represents the dissolved residual carbonate concentration in the effluent point after filtration, and $(CO_3^{2-})_t$ represents the total effluent carbonate levels without filtration, which determine both the dissolved residual carbonate and digested carbonate concentration from the sludge washed out from the reactor. An optimum operating condition is defined as the experimental parameter value resulting in the highest Crystallization Ratio (CR) value. A low CR value followed by a high Total Removal (TR) value indicates a significant amount of undesired sludge has formed in the system.

2.3.2 Analytical techniques

The concentration of each ion involved in the precipitation reaction in the effluent water was analyzed, and the carbonate treatment efficiency of the experiment was obtained. The calcium ion concentration was analyzed

using Inductively Coupled Plasma Mass Spectrometry (ICP-MS, Element 21, Thermo Scientific). High-resolution XRD (HR XRD, D8 DISCOVER, Bruker) was used to analyze the elemental components of the product. The XPS (ESCA, PHI 5000 Versa Probe, ULVAC-PHI) analyzed the chemical bonds contained in the product and provided qualitative and quantitative analyses of its constituents. The surface morphology of the particles was observed by a Thermal Field Emission SEM (FE-SEM, JSM-7800 F, Japan JEOL) to confirm the surface structure. In this way, the product's composition, purity, surface structure, and other characteristics are identified, based on which the suitability for use and recycling value of the resource-recycling product are determined.

3 Results and discussion

3.1 Influence of carbonate surface loading on carbonate removal and crystallization

Surface loading is the amount of carbonate that moves over a cross-sectional unit area (m^2) in a particular period (h) ($L, \text{kg m}^{-2} \text{h}^{-1}$). The amount of carbonate that crosses a cross-section area at a given time depends on the carbonate content in the initial influent at the stated

flow rate [21]. At these conditions, the influent MR of $[\text{Ca}^{2+}]/[\text{CO}_3^{2-}]=1.0$, the single influx flow rate= 50 mL min^{-1} , and the pH value of the system was held constant at 10. The carbonate surface loading varied from 14 to $69 \text{ kg m}^{-2} \text{h}^{-1}$.

As shown in Fig. 3, the carbonate removal and granulation efficiency were achieved at 97 and 96%, respectively, at the initial carbonate surface loading of $14 \text{ kg m}^{-2} \text{h}^{-1}$ and continued to decrease as the carbonate surface loading increased. When the surface load was continuously increased to $69 \text{ kg m}^{-2} \text{h}^{-1}$, the removal efficiency decreased to 88%, and the crystallization efficiency dropped to 80%. This reduces the likelihood that the initially generated nuclei will collide and disintegrate, thus lowering the crystallization efficiency [22]. At this juncture, the optimal conditions for easy operation and stable reactions were the carbonate surface loading of $55 \text{ kg m}^{-2} \text{h}^{-1}$, the influent carbonate concentration of 0.096 M resulting in a removal efficiency of 93%, and a crystallization efficiency of 84%.

Meanwhile, altering the carbonate surface loading flow rates used for recirculation affects the hydraulic retention time (HRT). An HRT of 9.0 min was calculated based

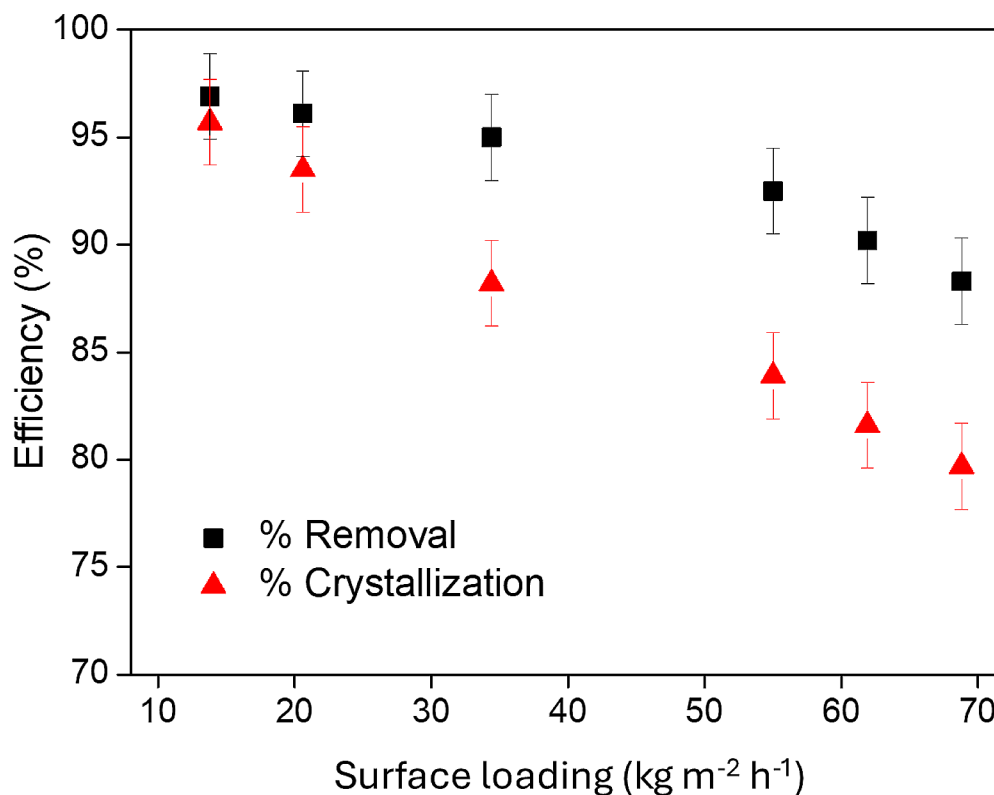


Fig. 3 Influence of carbonate surface loading on removal and crystallization efficiency

on the ratio of the primarily generated nuclei, which decreased the crystallization efficiency. The HRT was adjusted to optimize particle collision for the specified range of carbonate surface loadings [23]. A longer HRT is required to crystallize carbonate, which increases supersaturation and facilitates the formation of the amorphous material [24]. While increasing the surface loading creates a well-mixed environment to react adequately with the precipitating agent, it also increases the upward velocity that supports higher crystallization efficiency [25].

3.2 Influence of source of calcium ions on carbonate removal and crystallization

Variations in the calcium ion source can affect the removal and crystallization of carbonate from the synthetic flue gas absorbent solution. Two calcium sources were investigated to determine their influence on the system. $\text{Ca}(\text{OH})_2$ and $\text{Ca}(\text{NO}_3)_2$ were used for this purpose following the initial conditions provided. The influent concentration of carbonate was 0.096 M, with a carbonate surface loading of $55 \text{ kg m}^{-2} \text{ h}^{-1}$, and the pH value of the solutions was maintained constant between 10.0 and 10.3. The MR of $[\text{Ca}^{2+}]/[\text{CO}_3^{2-}]$ was controlled at 0.90, 0.95, 1.00, 1.05, 1.10 for a more detailed study.

The comparison between the two calcium ion sources determined which generated better carbonate removal and crystallization efficiency from the simulated flue gas absorbent liquid. The maximum removal of 95% at $[\text{Ca}^{2+}]/[\text{CO}_3^{2-}] = 1.05$ was achieved using calcium hydroxide, based on the calculations of the changing MRs (Fig. 4a). From MRs of $[\text{Ca}^{2+}]/[\text{CO}_3^{2-}]$ of 0.9 to 1.05, carbonate removal efficiency improved from 85 to 95%, but as MRs increased further to 1.1, carbonate removal tended to decrease to 86%. A similar pattern was observed when calcium nitrate was the source of calcium ions. An achievement of 86 to 98% was possible with a $[\text{Ca}^{2+}]/[\text{CO}_3^{2-}]$ MR of 0.9 to 1.05, while 94% was possible with an increased MR of 1.1. The maximum level of supersaturation that can impact the efficiency of removing carbonate was obtained by increasing the $[\text{Ca}^{2+}]/[\text{CO}_3^{2-}]$ MR [26, 27].

From Fig. 4b, it can be seen that with the $[\text{Ca}^{2+}]/[\text{CO}_3^{2-}]_{\text{MR}}$ of 1.05, the crystallization efficiency performed best at 85% when using calcium hydroxide and 97% when using calcium nitrate. Similarly, as the $[\text{Ca}^{2+}]/[\text{CO}_3^{2-}]_{\text{MR}}$ increased, the crystallization efficiency also increased. However, further increases in the $[\text{Ca}^{2+}]/[\text{CO}_3^{2-}]_{\text{MR}}$ tended to decrease the crystallization efficiency due to the excess amount of calcium ions that tend to dissolve, resulting in lower efficiency. Results showed that calcium nitrate yielded better results in the removal and crystallization efficiency of the carbonate crystals. The restricted supersaturation impacted the carbonate

precipitation processes in the reactor bed. At the reactant inflow, supersaturation was widespread and decreased as it rose in the reactor column. On the other hand, significant supersaturation required a liquid medium for the growth of new crystals, and more fines were also formed by spontaneous primary nucleation [24].

3.3 Influence of sulfate ion as interfering solutions

A sulfate ion was introduced to the influent solution to determine its influence on the removal and crystallization of the carbonate ions. The varying influent concentrations of sulfate ions, ranging from 10 to 50 mg L^{-1} , were calculated based on the concentration of sulfur oxides in the flue gas introduced to the system, while the other factors remained constant. The presence of sulfate in the solutions affects the crystallization process of calcium carbonate. Without sulfate ions in the solution, 98% carbonate removal and 97% crystallization efficiency were achieved. However, with increasing sulfate ion concentrations from 10 to 50 mg L^{-1} , carbonate removal insignificantly changed, while crystallization efficiency declined from 96 to 91% (Fig. 5). Two ions, hydroxide and sulfate, can compete with carbonate for calcium in solution for precipitation. Given the ideal operating condition for the molar ratio (MR) of $[\text{Ca}^{2+}]/[\text{CO}_3^{2-}]$ is 1.0, if calcium ions precipitate as other compounds, there will not be enough calcium ions for carbonate to carry out the crystallization reaction, leading to a decrease in carbonate removal efficiency. Sulfate also influences the treatment effectiveness through its ionic strength and crystal structure. Sulfate will be adsorbed onto the surface lattice of the calcium carbonate crystals formed in the FBR, replacing carbonate to combine with calcium ions and create calcium sulfate crystals. When all active sites are filled, the freshly formed calcium carbonate crystals either adhere to the remaining active sites or to the calcium sulfate crystals on the surface and continue growing. This is more likely to result in the formation of tiny crystals that readily wash out with the water flow, resulting in slower calcium carbonate formation and decreased crystallization efficiency [28, 29].

The pH of the system plays a significant role in determining the phases of metal and free ions. An increase in pH promotes the generation of OH^- ions, leading to the hydrolysis of free calcium and the formation of $\text{Ca}(\text{OH})_2$ begins to rise at pH 11.5. A diagram of the competition of $\text{Ca}(\text{OH})_2$ and CaCO_3 under the same initial concentration of Ca (0.096 M) was presented. As predicted in Fig. 6a, a further increase in pH augmented the levels of hydroxides which reduced the formation of CaCO_3 and shifted to the reactions of Ca^{2+} with hydroxides to form $\text{Ca}(\text{OH})_2$. Thus, the controlling pH below 11.5 was suggested to obtain a higher purity of recovered CaCO_3 .

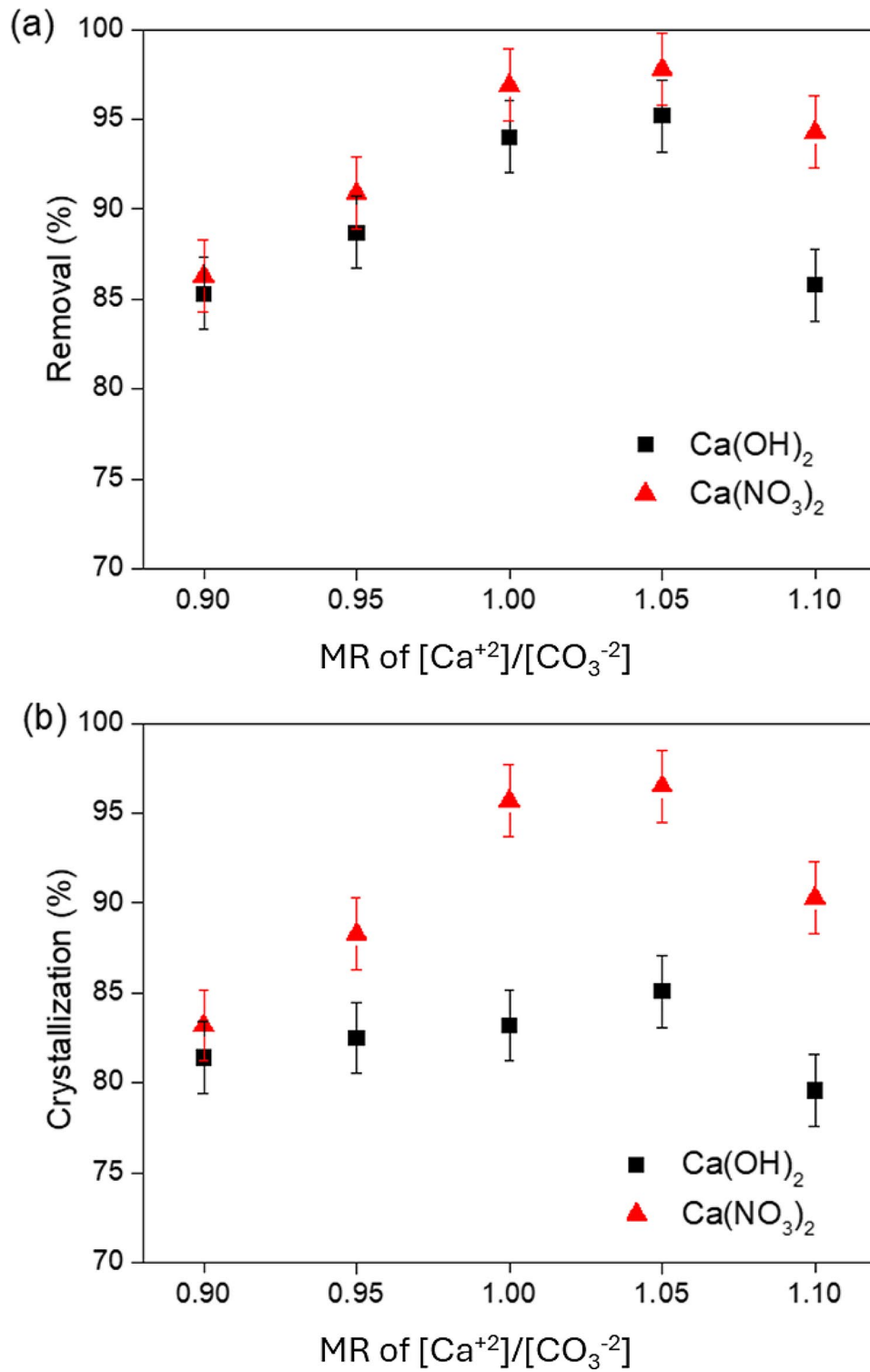


Fig. 4 Influence of calcium ion supply source on the carbonate (a) Removal and (b) Crystallization efficiency

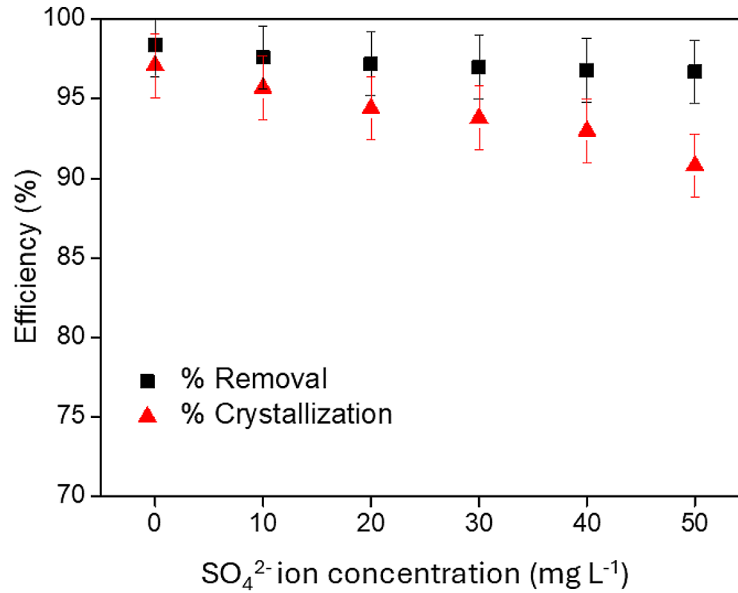
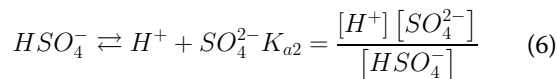
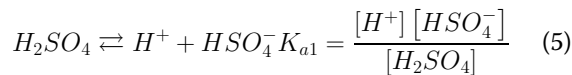


Fig. 5 Effect of sulfate concentration on carbonate removal and crystallization efficiency ($[\text{CO}_3^{2-}] = 0.096 \text{ M}$; $[\text{Ca}^{2+}] = 0.096 \text{ M}$; $\text{pH} = 10$; carbonate surface loading $55.0 \text{ kg m}^{-2} \text{ h}^{-1}$)

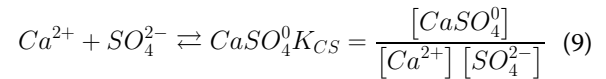
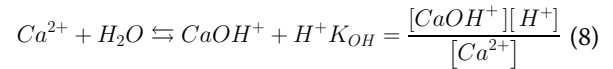
pH is also indisputably related to the crystallization processes of sulfate species in solution. There are two different K_a values for the dissociation of protons in phosphoric acid: $K_{a1} = 10^3$, $K_{a2} = 1.2 \times 10^{-2} \text{ M}$ (Eqs. (5) and (6)). Correspondingly, their ionization equations and equilibrium constants are expressed as follows:



Based on Eqs. (7) and (8), the total sulfate concentration can be determined by summing up the concentrations of these species.

$$[\text{SO}_4^{2-}]_T = [\text{SO}_4^{2-}] + [\text{HSO}_4^-] + [\text{H}_2\text{SO}_4] \quad (7)$$

Theoretical considerations suggest that changing the pH can alter the species distribution of calcium, carbonate, and sulfate, potentially affecting the prevalent reactions in the system. There are two kinds of calcium species in $\text{Ca-H}_2\text{O-SO}_4^{2-}$ system such as CaOH^+ ($K_{\text{OH}} = 10^{-12.7} \text{ M}$) and CaSO_4 ($K_{\text{CS}} = 10^{2.36} \text{ M}$). Correspondingly, their equilibrium equations and cumulative formation constant are expressed as follows Eqs. (9, 10 and 11):



In term of $[\text{Ca}^{2+}]$, the two species of Ca existing in solution are as follows:

$$[\text{Ca}^{2+}]_T = [\text{Ca}^{2+}] + [\text{CaOH}^+] + [\text{CaSO}_4^0] \quad (10)$$

$$[\text{Ca}^{2+}]_T = [\text{Ca}^{2+}] \left(1 + \frac{K_{\text{OH}}}{[\text{H}^+]} + K_{\text{CS}} [\text{SO}_4^{2-}] \right) \quad (11)$$

Therefore, the existence of sulfate strongly affects CaCO_3 granulation due to the formation of CaSO_4 complex in solution. As presented in Fig. 6b, a higher initial sulfate concentration results in a lower formation of CaCO_3 , consistent with the results of carbonate removal presented in Fig. 5. When sulfate is present at a concentration of 50 mg L^{-1} , the efficiency of calcium removal decreases. Initially, at a sulfate concentration of 10 mg L^{-1} , the removal rates were approximately 98% for TR and 96% for CR. However, as the sulfate concentration increased to 50 mg L^{-1} , these efficiencies reduced to 97% for TR and 91% for CR, significantly impacting the crystallization efficiency. Meanwhile, Ca(OH)_2 only shows an

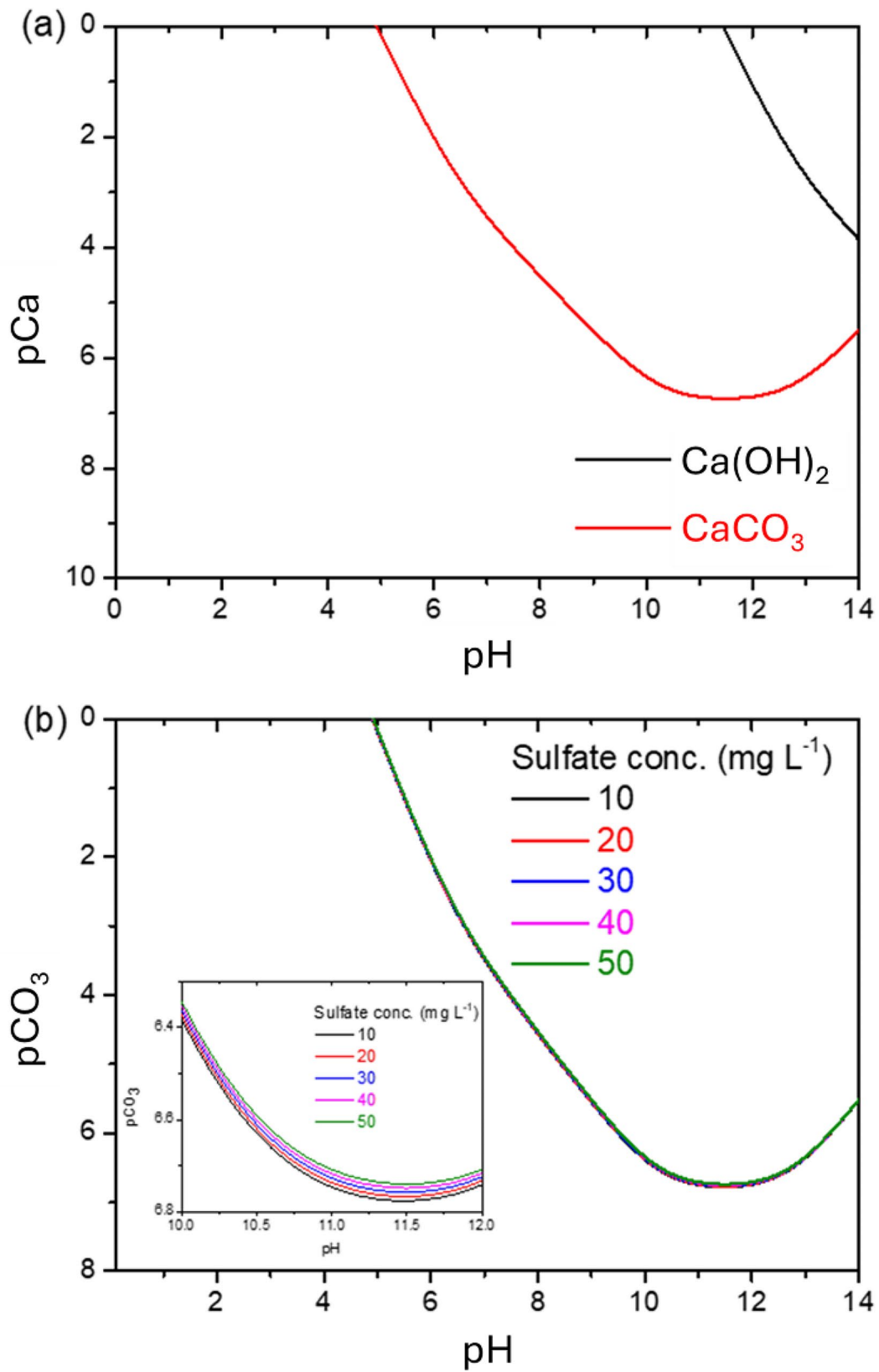


Fig. 6 (a) Ca(OH)_2 and CaCO_3 solubility curve versus pH ($[\text{Ca}]_0 = 0.096 \text{ M}$) and (b) CaCO_3 solubility curve under different existence of sulfate concentration ($[\text{Ca}]_0 = 0.096 \text{ M}$, $[\text{SO}_4]_0 = 10\text{--}50 \text{ mg L}^{-1}$)

effect on the recovery of CaCO_3 under extremely alkaline conditions.

3.4 Calcium carbonate crystal characterization

The product with a surface loading of $69 \text{ kg m}^{-2} \text{ h}^{-1}$ was sieved with sieve apertures of 0.355 mm and 0.7 mm for SEM and XRD analysis to understand the growth mechanism of the crystalline particle product. Simultaneously, the crystalline particles at surface loadings of $69 \text{ kg m}^{-2} \text{ h}^{-1}$ and $55.0 \text{ kg m}^{-2} \text{ h}^{-1}$ were chosen for SEM and XRD investigation to examine the impact of carbonate surface loading on the product's surface structure.

The crystallization process showed a positive correlation between the product's particle size and HRT. In Fig. 7a, it can be observed that the initially generated nuclei transformed into fine crystals with sharp edges and corners. Upon magnification, the crystal structure present on its surface became clearer at 150 times magnification. As they bonded, the newly formed crystals clustered together, reducing their angularity and causing them to aggregate. At 110 times magnification, larger particles were produced simultaneously by attaching new crystals to the spaces between the smaller ones (Fig. 7b). The particle size increased compared to Fig. 7a. Lastly, in Fig. 7c, the crystals were observed at 55 times

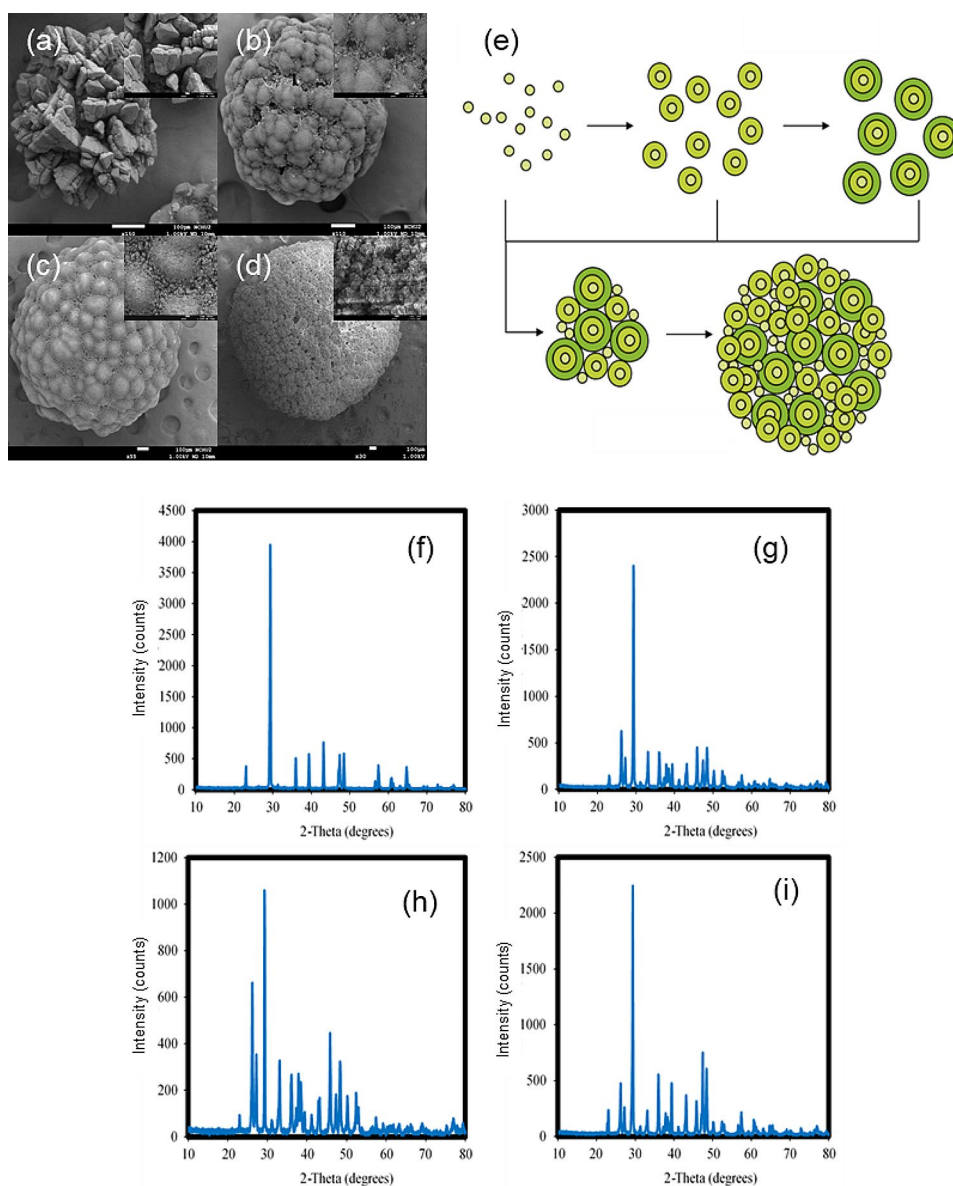


Fig. 7 SEM analysis of the crystal product at surface loading = $6.9 \text{ kg m}^{-2} \text{ h}^{-1}$, (a) $< 0.355 \text{ mm}$, (b) $0.355\text{--}0.7 \text{ mm}$, (c) $> 0.7 \text{ mm}$, (d) at surface loading = $55 \text{ kg m}^{-2} \text{ h}^{-1}$ at $> 0.7 \text{ mm}$. (e) a schematic diagram of the layered growth of crystals. XRD analysis of crystals at surface loading = $6.9 \text{ kg m}^{-2} \text{ h}^{-1}$, (f) $< 0.355 \text{ mm}$, (g) $0.355\text{--}0.7 \text{ mm}$, (h) $> 0.7 \text{ mm}$, (i) at surface loading = $55 \text{ kg m}^{-2} \text{ h}^{-1}$ at $> 0.7 \text{ mm}$

magnification, resembling the structure of Fig. 7b, with further enhanced smoothness and particle size visible at 30 times magnification (Fig. 7d). The final output is smoother than the first two crystals, even if it is not perfectly spherical.

As depicted in Fig. 7e, an illustration of the layered formation of crystals is evident. In the FBR's reaction zone, tiny crystals initially formed. As fine crystal formations persisted, a crystal layer gradually developed and connected, increasing the particle size. With an extended reaction period during continuous crystallization, the nuclei grouped to form larger aggregates. As the crystallization reaction occurred on the surface of the particles, the particle size gradually increased. However, once the crystal particles reached a specific size, they collided appreciably due to their weight and hydraulic circumstances, causing them to become fluidized in the FBR.

The results of the XRD study are shown in Fig. 7g and i. The peak characteristics provided were consistent with the reference depicted in Fig. 7f. The XRD analysis was conducted at a surface loading of $6.9 \text{ kg m}^{-2} \text{ h}^{-1}$ for granules of different sizes, and the highest crystalline phase of CaCO_3 was observed when the particle size of the product was less than 0.35 mm. It was evident that the obtained product primarily contained calcium carbonate [30, 31]. Consequently, the calcium carbonate crystals produced in the reaction zone initially had a high degree of purity as the reaction period increased. It is possible that the other ions from the reaction were adsorbed onto the product's surface, which increased the crystal particle size. The three samples contained consistent and distinct characteristic peaks at 29, 39, 46, and 48°, demonstrating that the substance was calcium carbonate when compared to the calcium carbonate standard product through XRD analysis.

The crystal products generated at a pH of 10 were examined using XPS analysis. Analysis of Fig. 8a and b demonstrated that no calcium hydroxide was developed under this condition. The decomposition results of the two figures showed that the analysis results of calcium and oxygen in XPS can be attributed entirely to calcium carbonate peaks. The reaction region indicated that calcium carbonate constituted the majority of the composition. It was confirmed that these conditions would not lead to the formation of calcium hydroxide and a reduction in carbonate treatment effectiveness.

Figure 8c and d displayed the findings of the XPS results of calcium and oxygen at pH 11 crystal product. The peak regions in Fig. 8c were divided into peaks according to the binding energy (BE) and the orbital areas that correspond to the potential products that could develop and be degraded. The four peaks $\text{Ca(OH)}_2 2p_{3/2}$, $\text{CaCO}_3 2p_{3/2}$, $\text{Ca(OH)}_2 2p_{1/2}$, and $\text{CaCO}_3 2p_{1/2}$ were identified. Following the same pattern, $\text{Ca(OH)}_2 1s$ and

$\text{CaCO}_3 1s$ were split into two peaks. By putting the calcium hydroxide and calcium carbonate peak regions in the same orbital region and comparing them, the product components can be quantified to estimate the percentage of each content (Fig. 8d). The results showed that the pH of 11 crystal products had an approximate 2.6:1 calcium carbonate to calcium hydroxide concentration ratio.

Figure 8e and f showed the findings of the XPS examination of calcium and oxygen at a pH of 12. Figure 8e was broken into four separate peaks: $\text{CaCO}_3 2p_{3/2}$, $\text{Ca(OH)}_2 2p_{3/2}$, $\text{CaCO}_3 2p_{1/2}$, and $\text{Ca(OH)}_2 2p_{1/2}$. Figure 8f was also degraded into two peaks of $\text{CaCO}_3 1s$ and $\text{Ca(OH)}_2 1s$. To quantify the product components, the area of each peak was sorted, compared, and the proportion was examined. According to the findings, the pH of 12 products had a calcium carbonate to calcium hydroxide concentration ratio of roughly 1.1:1. It was confirmed that each peak's BE values are within the range of calcium carbonate's matching elemental binding energy peaks and orbitals in the reference and NIST XPS databases. This proved the product's composition was calcium carbonate [32–34].

The use of calcium, magnesium, and barium in the recent papers for carbon sequestration is compared in Table 3. Ca^{2+} was the common precipitant to promote carbonate removal through chemical precipitation in early works. However, conventional precipitation treatment created a large amount of water-rich sludge that needed further dewatering. As illustrated in Table 3, CaCO_3 recycling using the expanded granular sludge bed process could produce granules; however, a long time was required to have an efficient operating time. Thus, FBHC used in this study is an economical and highly feasible method of treatment due to its short reaction time, neutral pH reaction, and the production of large granule products that are suitable for further use.

3.5 Economic analysis

A cost-benefit analysis was performed to assess the economic advantages of using the FBR system for treating wastewater with high carbonate content. The FBR system stands out for its ability to reduce sludge and create valuable pellets, leading to lower solid waste disposal costs compared to traditional chemical precipitation. Both systems use equal amounts of chemicals.

With a carbonate concentration of 5760 mg L^{-1} in the wastewater, treating 1000 L allows for the recovery of 5356 g of carbonate, equivalent to 8.92 kg of CaCO_3 . Disposal costs in Taiwan are roughly $\$0.16 \text{ kg}^{-1}$ solid [35]. Traditional methods recover solids as sludge, with costs around $\$8.92 \text{ m}^{-3}$, considering an average water content of 84% in the sludge [36], leading to a total sludge mass of 55.8 kg. The FBR system, however, separates 8.06 kg as pellets and 0.86 kg as sludge, with significantly different water contents of 5 and 84%, respectively. This results in

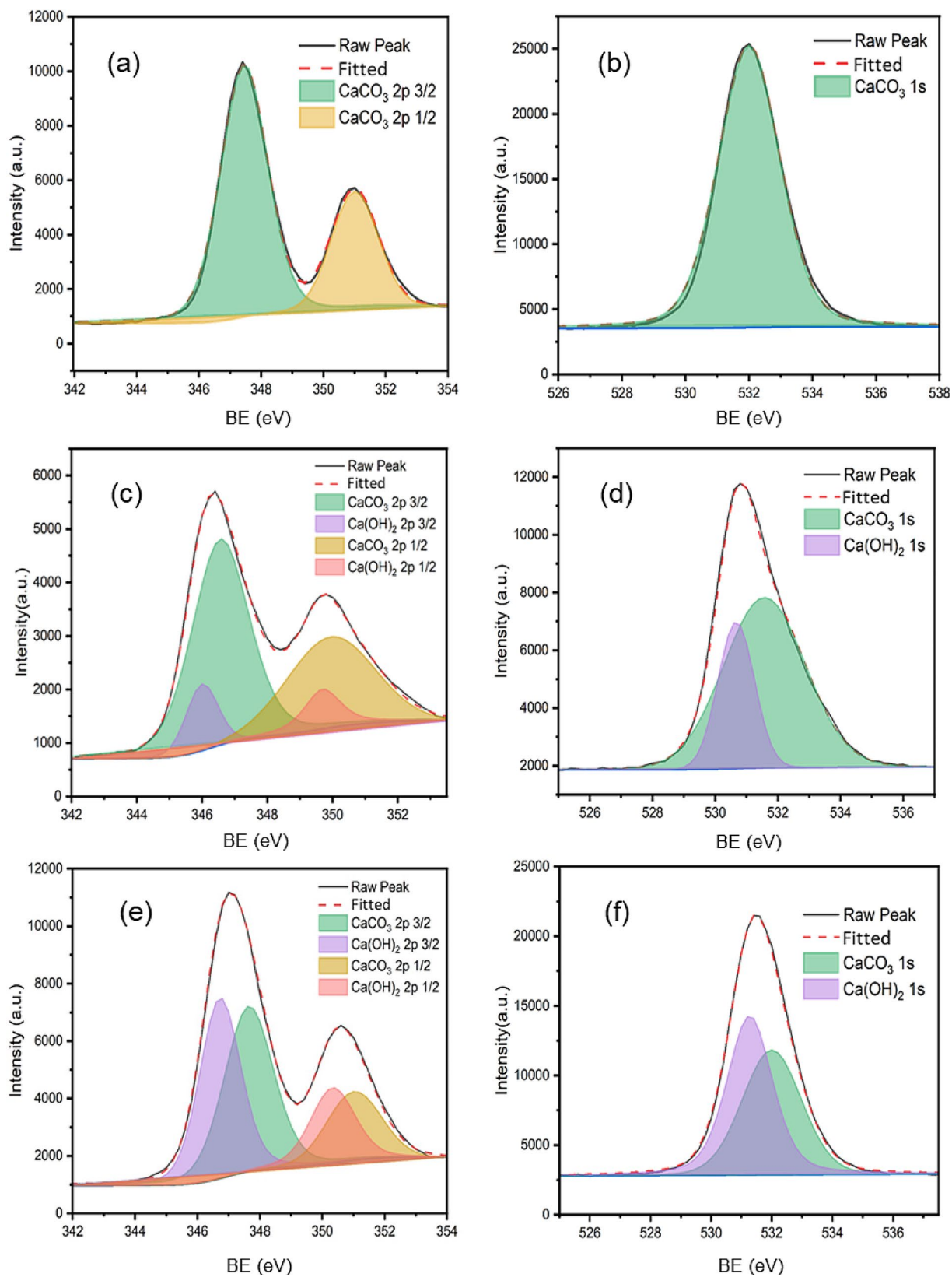


Fig. 8 The XPS analysis of (a) Calcium element, (b) Oxygen element at pH of 10, (c) Calcium element, (d) Oxygen element at pH of 11, (e) Calcium element, (f) Oxygen element at pH of 12

Table 3 Comparison of carbon sequestration by using precipitant salts

Reactant	Methods	Product	Conditions	Product size	Ref.
Mg ²⁺	Fluidized-bed	Granule of MgCO ₃	[Mg] ₀ = 2046 mg L ⁻¹ , pH = 11.3, Time = 3–5 d	Size > 1 mm	[37]
	Chemical Precipitation	Sludge of amorphous MgCO ₃	[Mg] ₀ = 4,800 mg L ⁻¹ , pH 9.0, time = 5 h	-	[38]
Ba ²⁺	Chemical Precipitation	Sludge of amorphous BaCO ₃	[Ba] ₀ = 16,470 mg L ⁻¹ , pH > 10, time = 2 h	Size < 10 μm	[39]
			[Ba] ₀ = 5206 mg L ⁻¹ , pH 9.0–10.5, time = 90 min	Size < 200 μm	[40]
			[Ba] ₀ = 27,400 mg L ⁻¹ , pH 9.6–12.0, time = 90 min	Size < 3 μm	[41]
Ca ²⁺	Expanded granular sludge bed	Granule of CaCO ₃	[CO ₃] ₀ = 1200 mg L ⁻¹ , pH = 10.5, Time = 70 d	Size > 0.5 mm	[42]
	Chemical Precipitation	Sludge of amorphous CaCO ₃	[Ca] ₀ = 4000–8000 mg L ⁻¹ , pH 10.0, Time = 180 min	Size < 10 μm	[43]
			pH > 10.0, Time = 180 min	Size < 10 μm	[44]
			[Ca] ₀ = 72,072 mg L ⁻¹ , pH 12.0, Time = 60 min	Size < 30 μm	[45]
			[Ca] ₀ = 2000–4000 mg L ⁻¹ , pH 9.0, Time = 300 min	Size < 5 μm	[46]
			[Ca] ₀ = 3840 mg L ⁻¹ , pH 10.0, Time = 7 d	Size > 1 mm	This study

a lower disposal cost of about \$2.2 m⁻³. The FBR system not only cuts disposal costs but also requires less space than conventional methods. Moreover, the recovered pellets can be post-treated and reused. These factors make FBR an economically attractive option for future wastewater treatment. However, FBHC faces challenges including the cost of continuous flow control, scalability issues like fouling and agglomeration, and the need to address the disposal and treatment of toxic by-products.

4 Conclusions

To recover the carbonate ions after simulating potassium hydroxide absorption, FBHC technology was evaluated. The effect of different Ca sources, surface loading, and interference ions such as sulfate was conducted to optimize the crystallization of recovered calcium carbonate. The capacity of the FBHC system was maximized at a cross-sectional loading of 55 kg m² h⁻¹ and pH 10.0, resulting in a crystallization efficiency of 85% with a corresponding total removal efficiency of 98%. Based on XRD and XPS analysis, the pellet product was identified as CaCO₃, indicating high purity. Meanwhile, the reduction in solid disposal costs from 8.93 to 2.20 US\$ can be considered as one of the economic potentials of applying FBR in carbon sequestration from wastewater. The CO₂ in the atmosphere absorbed by the flue gas can be recovered as granulated pellets through fluidized-bed crystallization, which is highly separable and has high potential for further use. FBHC technology offers a promising solution for industries to reduce CO₂ emissions, particularly in power generation and heavy industries like cement and steel, thereby aiding compliance with environmental

regulations and contributing to global emission reduction efforts.

Acknowledgements

The authors would like to thank the Ministry of Science and Technology (110-2622 - E - 005-015) for their support through funding this research. The support of SEM, XRD and XPS measurements from The Instrument Center of National Chung Hsing University is greatly acknowledged.

Author contributions

Po-Chun Huang carries out the methodology, formal analysis, and investigation of the study. Anabella C. Vilando facilitate on the Validation, review and editing. Thi-Hanh Ha participated in the methodology and visualization. Ming-Chun Lu participated in conceptualization, resources, supervision, project administration, and funding acquisition. All authors read and approved the final manuscript.

Funding

This work was financially supported by the "Innovative Center on Sustainable Negative-Carbon Resources" from the Featured Areas Research Center Program within the Higher Education Sprout Project framework by the Ministry of Education (MOE) in Taiwan. The Ministry of Science and Technology of Taiwan also supported this research under Contract Number MOST 110-2622 -E - 005-015.

Data availability

All data generated or analyzed during this study are available upon request to the corresponding author.

Declarations

Competing interests

The authors declare they have no competing interests.

Received: 11 November 2023 / Accepted: 8 May 2024

Published online: 13 June 2024

References

- USEPA. Climate Change Indicators: Greenhouse Gases. Washington, DC: United States Environmental Protection Agency; 2024. <https://www.epa.gov/climate-indicators/greenhouse-gases> (Accessed 15 Apr 2024).
- Ben Miloud HM and Ashargawi AS. An analysis study on the effect of increasing carbon dioxide gas and climate change on temperatures in Libya. *J Sol Energy Sustain Dev*. 2023;12:4–11.
- Friedlingstein P, O'Sullivan M, Jones MW, Andrew RM, Gregor L, Hauck J, et al. Global carbon budget 2022. *Earth Syst Sci Data*. 2022;14: 4811–900.
- Hassan A. The likely irreversible catastrophe of global warming and human ignorance. Geneva: Zenodo; 2023. <https://doi.org/10.5281/zenodo.7878377>. (Accessed 26 Apr 2024)
- UNFCCC. the 27th Conference of the Parties to the United Nations Framework Convention on Climate Change. Bonn: the United Nations Framework Convention on Climate Change; 2022. <https://unfccc.int/cop27> (Accessed 15 Apr 2024).
- IPCC. Climate Change 2013: The Physical Science Basis. Geneva: Intergovernmental Panel on Climate Change; 2013. <https://www.ipcc.ch/report/ar5/wg1/> (Accessed 15 Apr 2024).
- Lau HC, Tsai SC. A decarbonization roadmap for Taiwan and its energy policy implications. *Sustainability*. 2022;14:8425.
- Zhang Z, Huisin D. Carbon dioxide storage schemes: Technology, assessment and deployment. *J Clean Prod*. 2017;142:1055–64.
- Vadillo JM, Gomez-Coma L, Garea A, Irabien A. Non-dispersive CO₂ separation process using vacuum desorption and ionic liquids as carbon capture and utilization innovative technology. *Sep Purif Technol*. 2022;301:121923.
- Huang YH, Garcia-Segura S, de Luna MDG, Sioson AS, Lu MC. Beyond carbon capture towards resource recovery and utilization: fluidized-bed homogeneous granulation of calcium carbonate from captured CO₂. *Chemosphere*. 2020;250:126325.
- Zhang T, Ding L, Ren H. Pretreatment of ammonium removal from landfill leachate by chemical precipitation. *J Hazard Mater*. 2009;166:911–5.
- Ha TH, Mahasti NNN, Lu MC, Huang YH. Application of low-solubility dolomite as seed material for phosphorus recovery from synthetic wastewater using fluidized-bed crystallization (FBC) technology. *Sep Purif Technol*. 2022;303:122192.
- Ha TH, Mahasti NNN, Lin CS, Lu MC, Huang YH. Enhanced struvite (MgNH₄PO₄·6H₂O) granulation and separation from synthetic wastewater using fluidized-bed crystallization (FBC) technology. *J Water Process Eng*. 2023;53:103855.
- Salcedo AFM, Ballesteros FC, Vilando AC, Lu MC. Nickel recovery from synthetic Watts bath electroplating wastewater by homogeneous fluidized bed granulation process. *Sep Purif Technol*. 2016;169:128–36.
- Vilando AC, Caparanga AR, Lu MC. Enhanced recovery of aluminum from wastewater using a fluidized bed homogeneously dispersed granular reactor. *Chemosphere*. 2019;223:330–41.
- de Luna MDG, Capito JA, Vilando AC, Lu MC. Effect of EDTA and CH₂O on copper recovery from simulated electroless copper plating spent rinse water by unseeded fluidized-bed granulation process. *Sep Purif Technol*. 2020;253:117460.
- Smirnova N, Demyan MS, Rasche F, Cadisch G, Müller T. Calibration of CO₂ trapping in alkaline solutions during soil incubation at varying temperatures using a Respicond VI. *Open J Soil Sci*. 2014;4:161–7.
- Coker AK. Ludwig's Applied Process Design for Chemical and Petrochemical Plants. 4th ed. Boston: Gulf Professional Publishing; 2010.
- amiliani UN, Purba E. Purification of biogas by CO₂ reduction in biogas using potassium hydroxide solution (KOH) in a packed tower. *Adv Eng Res*. 2021;202:314–7.
- de Luna MDG, Sioson AS, Choi AES, Abarca RRM, Huang YH, Lu MC. Operating pH influences homogeneous calcium carbonate granulation in the frame of CO₂ capture. *J Clean Prod*. 2020;272:122325.
- Vilando AC, Caparanga AR, Huang YH, Lud MC. Tohdite recovery from water by fluidized-bed homogeneous granulation process. *Desalin Water Treat*. 2017;96:224–30.
- Liu PC, Vilando AC, Lu MC. Treatment of synthetic zinc and nickel wastewater and identification of its crystallization products by fluidized bed homogeneous crystallization technology. *Process Saf Environ*. 2022;164:154–63.
- Guevara HPR, Ballesteros FC, Vilando AC, de Luna MDG, Lu MC. Recovery of oxalate from bauxite wastewater using fluidized-bed homogeneous granulation process. *J Clean Prod*. 2017;154:130–8.
- Quimada NE, De Luna MDG, Vilando AC, Lu MC. Competitive effect of copper and nickel recovery with carbonate in the fluidized-bed homogeneous granulation process. *Environ Sci Pollut R*. 2022;29:12414–26.
- de Luna MDG, Bellotindos LM, Asiao RN, Lu MC. Removal and recovery of lead in a fluidized-bed reactor by crystallization process. *Hydrometallurgy*. 2015;155:6–12.
- Tiangco KAA, de Luna MDG, Vilando AC, Lu MC. Removal and recovery of calcium from aqueous solutions by fluidized-bed homogeneous crystallization. *Process Saf Environ*. 2019;128:307–15.
- Boonrattanakij N, Puangsuwan S, Vilando AC, Lu MC. Influence of coexisting EDTA, citrate, and chloride ions on the recovery of copper and cobalt from simulated wastewater using fluidized-bed homogeneous granulation process. *Process Saf Environ*. 2023;172:83–96.
- Tang Y, Zhang F, Cao Z, Jing W, Chen Y. Crystallization of CaCO₃ in the presence of sulfate and additives: Experimental and molecular dynamics simulation studies. *J Colloid Interf Sci*. 2012;377:430–7.
- Yan Y, Yu T, Zhang H, Song J, Qu C, Li J, et al. Co-deposition mechanisms of calcium sulfate and calcium carbonate scale in produced water. *Crystals*. 2021;11:1494.
- Sahebian S, Zebarjad SM, Sajjadi SA, Sherafat Z, Lazzeri A. Effect of both uncoated and coated calcium carbonate on fracture toughness of HDPE/CaCO₃ nanocomposites. *J Appl Polym Sci*. 2007;104:3688–94.
- Reis MC, Sousa MFB, Alobaid F, Bertran CA, Wang Y. A two-fluid model for calcium carbonate precipitation in highly supersaturated solutions. *Adv Powder Technol*. 2018;29:1571–81.
- Baer DR, Moulder JF. High-resolution XPS spectrum of calcite (CaCO₃). *Surf Sci Spectra*. 1993;2:1–7.
- Demri B, Muster D. XPS study of some calcium compounds. *J Mater Process Tech*. 1995;55:311–4.
- Zhang W, Li X, Qu Z, Zhao Q, Chen G. Facile solution synthesis and characterization of CaCO₃ microspheres with urchin-shaped structure. *Mater Lett*. 2010;64:71–3.
- Lin JY, Mahasti NNN, Huang YH. Fluidized-bed crystallization of barium perborate for continuous boron removal from concentrated solution: Supersaturation as a master variable. *Sep Purif Technol*. 2021;278:119588.
- Mahasti NNN, Shih YJ, Vu XT, Huang YH. Removal of calcium hardness from solution by fluidized-bed homogeneous crystallization (FBHC) process. *J Taiwan Inst Chem E*. 2017;78:378–85.
- Le VG, Vo DVN, Tran HT, Duy Dat N, Luu SDN, Rahman MM, et al. Recovery of magnesium from industrial effluent and its implication on carbon capture and storage. *ACS Sustain Chem Eng*. 2021;9:6732–40.
- Zhu C, Wang H, Li G, An S, Ding X, Teng HH, et al. CO₂ absorption and magnesium carbonate precipitation in MgCl₂-NH₃-NH₄Cl solutions: implications for carbon capture and storage. *Minerals*. 2017;7:172.
- Park S, Bang JH, Song K, Jeon CW, Park J. Barium carbonate precipitation as a method to fix and utilize carbon dioxide. *Chem Eng J*. 2016;284:1251–8.
- Arenas C, Ricaurte L, Figueredo M, Cobo M. CO₂ capture via barium carbonate formation after its absorption with ammonia in a pilot scale column. *Chem Eng J*. 2014;254:220–9.
- Gaur A, Park JW, Jang JH, Song HJ. Precipitation of barium carbonate from alkanolamine solution—study of CO₂ absorption from landfill gas (LFG). *J Chem Technol Biot*. 2011;86:153–6.
- Liu X, Pan D, Yuan Q, Feng X, Li M, Song X, et al. Anaerobic granular sludge performance in an expanded granular sludge bed reactor treating calcium-rich wastewater by adjusting CaCO₃ crystallization: Effect of upflow velocity and Ca²⁺ concentration. *Sci Total Environ*. 2024;912:169064.
- Mei X, Zhao Q, Li Y, Min Y, Liu C, Saxen H, et al. Phase transition and morphology evolution of precipitated calcium carbonate (PCC) in the CO₂ mineralization process. *Fuel*. 2022;328:125259.
- Zhao T, Guo B, Zhang F, Sha F, Li Q, Zhang J. Morphology control in the synthesis of CaCO₃ microspheres with a novel CO₂-storage material. *ACS Appl Mater Inter*. 2015;7:15918–27.
- Tan WL, Tan HF, Ahmad AL, Leo CP. Carbon dioxide conversion into calcium carbonate nanoparticles using membrane gas absorption. *J CO₂ Util*. 2021;48:101533.

46. Heuer J, Kraus Y, Vucak M, Zeng AP. Enhanced sequestration of carbon dioxide into calcium carbonate using pressure and a carbonic anhydrase from alkaliphilic *Coleofasciculus chthonoplastes*. *Eng Life Sci.* 2022;22:178–91.

Publisher's Note

Springer Nature remains neutral with regard to jurisdictional claims in published maps and institutional affiliations.